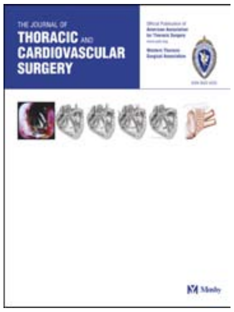

Is it Possible to Assess the Best Mitral Valve Repair in The Individual Patient? Preliminary Results of a Finite Element Study from Magnetic Resonance Imaging Data

Francesco Sturla , MSc Francesco Onorati , MD PhD Emiliano Votta , PhD Konstantinos Pechlivanidis , MD Marco Stevanella , PhD Aldo D. Milano , MD Giovanni Puppini , MD Alessandro Mazzucco , MD Alberto Redaelli , PhD Giuseppe Faggian , MD.

PII: S0022-5223(14)00734-X

DOI: 10.1016/j.jtcvs.2014.05.071

Reference: YMTC 8652

To appear in: *The Journal of Thoracic and Cardiovascular Surgery*

Received Date: 9 April 2014

Revised Date: 21 May 2014

Accepted Date: 27 May 2014

Please cite this article as: Sturla F, Onorati F, Votta E, Pechlivanidis K, Stevanella M, Milano AD, Puppini G, Mazzucco A, Redaelli A, Faggian G, Is it Possible to Assess the Best Mitral Valve Repair in The Individual Patient? Preliminary Results of a Finite Element Study from Magnetic Resonance Imaging Data, *The Journal of Thoracic and Cardiovascular Surgery* (2014), doi: 10.1016/j.jtcvs.2014.05.071.

Is it Possible to Assess the Best Mitral Valve Repair in The Individual Patient? Preliminary Results of a Finite Element Study from Magnetic Resonance Imaging Data

Francesco Sturla[1,2], MSc, Francesco Onorati[1], MD PhD, Emiliano Votta[2], PhD, Konstantinos Pechlivanidis[1], MD, Marco Stevanella[2], PhD, Aldo D. Milano[1], MD, Giovanni Puppini[3], MD, Alessandro Mazzucco[1], MD, Alberto Redaelli[2], PhD, Giuseppe Faggian[1] , MD.

[1] Division of Cardiovascular Surgery, Università degli Studi di Verona, Italy

[2] Department of Electronics, Informatics and Bioengineering, Politecnico di Milano, Italy

[3] Department of Radiology, Università degli Studi di Verona, Italy

Corresponding Author:

Francesco Sturla

PhD Program in Cardiovascular Sciences, University of Verona Medical School

Department of Electronics, Informatics and Bioengineering, Politecnico di Milano

Via Golgi 39, 20133 Milano

Italy

Phone: +39-02-2399-3327

fax: +39-02-2399-3360

email: francesco.sturla@univr.it; francesco.sturla@mail.polimi.it

Category: Evolving Technology/Basic Science

Manuscript word count: 3883

ABSTRACT

Objectives: Finite element modeling was adopted to quantitatively compare, for the first time and on a patient-specific basis, the biomechanical effects of a broad spectrum of different neochordal implantation techniques for the repair of isolated posterior mitral leaflet prolapse.

Methods: Cardiac magnetic resonance images were acquired on four patients undergoing surgery. The patient-specific three-dimensional model of mitral apparatus, and the motion of annulus and papillary muscles were reconstructed: location and extent of the prolapsing region were confirmed by intraoperative findings and the mechanical properties of mitral leaflets, chordae tendineae and expanded polytetrafluoroethylene neochordae were included. Mitral systolic biomechanics was finally simulated in preoperative conditions and following five different neochordal procedures: single neochorda, double neochorda, "standard" neochordal loop with three neochordae of the same length and two "pre-measured" loops with one common neochordal loop, and three different branched neochordae arising from it, alternatively of 1/3 and 2/3 of the entire length.

Results: The "best" repair in terms of biomechanics was achieved with a specific neochordal technique in the single patient, according to the location of the prolapsing region. However, all techniques achieved slight reduction of papillary muscles forces and tension relief of intact native chordae proximal to the prolapsing region. Multiple neochordae implantation improved the repositioning of the prolapsing region below the annular plane and better redistributed mechanical stresses on the leaflet.

Conclusions: Although applied on a small cohort of patients, systematic biomechanical differences were noticed between neochordal techniques, potentially affecting their short-to-long term clinical outcome. This study opens the way to patient-specific optimization of neochordal techniques.

ULTRAMINI ABSTRACT

Finite element analysis was used to quantitatively compare, on a patient-specific basis, the biomechanical effects of a broad spectrum of different neochordal implantation techniques for the repair of mitral posterior leaflet prolapse. Systematic biomechanical differences between neochordal techniques were noticed, potentially affecting clinical outcome.

Abbreviations and acronyms

cMRI = cardiac magnetic resonance imaging

CoA = coaptation area

CoL = coaptation length

DN = double neochordal implantation

ePTFE = expanded polytetrafluoroethylene

F_{ePTFE} = artificial suture tension

F_{nc} = natice chordal tension

F_{PM} = papillary muscles forces

FE = finite element

FED = fibroelastic deficiency

IPP = isolated posterior leaflet prolapse

MV = mitral valve

LN = non-standard pre-measured neochordal implantation with common loop of 1/3 of the entire length

LNH = non-standard pre-measured neochordal implantation with common loop of 2/3 of the entire length

NCI= neochordal implantation

PM = papillary muscle

Pre-model = preoperative model

Phys-model = physiological model

SL = standard loop implantation

SN = single neochordal implantation

S_I = maximum principal stress

S_I^{MAX} = peak value of maximum principal stresses along the leaflet free margin

INTRODUCTION

Degenerative MV prolapse represents the most common mitral disease in western Countries.[1] Posterior leaflet prolapse is the most common pathologic feature of degenerative MV, with several conservative surgical techniques popularized during the decades, the first of which dates back to 1983.[2] However, recent studies have demonstrated comparable clinical outcome, together with potential superior results in terms of physiology, with techniques able to respect rather than resect the diseased portion of the mitral valve.[3] Most of those techniques rely on the use of neochordal implantation (NCI), whose principal drawback is related to the precise assessment of neochordal length during surgical intervention.[4,5] For that reason, several techniques have been employed for the correct measurement of neochordal length, fundamentally based on *in-vivo* beating-heart anatomical measurement with transesophageal echocardiography[6] or *in-vivo* "standstill-heart" functional measurement with intermittent saline injection.[7] Furthermore, single[8] or multiple neochordal stitching have been reported.[9] All these techniques have been proved effective in the relief of MV prolapse and associated with excellent mid-to-long term outcome.[10]

Although in the last few decades FE modeling has been increasingly adopted to study mitral valve and quantify its biomechanics, both in physiological and pathological conditions[11], few literature studies have tried to address the impact of NCI on MV biomechanics through FE technique.[12-14,] Indeed, a pioneer study was performed by Kunzelman and colleagues[13] on a paradigmatic MV model, derived from porcine fresh hearts. A more recent study[14] overcomes the shortcomings of previous paradigmatic FE models, via a computational protocol able to virtually simulate the effects of increasing number of artificial sutures, although based on a single MV geometry.

However, no study has ever investigated the biomechanics underlying the above-mentioned spectrum of different surgical NCI techniques and, in particular, using a patient-specific multidisciplinary approach combining bioengineer, radiological and surgical methods. Therefore it was the aim of this study to deeper investigate degenerative MVs with isolated P2-scallop prolapse via a computational evaluation protocol, based on FE method combining patient-specific MV modeling from cardiac magnetic resonance imaging (cMRI) and intraoperative surgical findings, in order to assess biomechanical effects of different clinical scenarios of P2-prolapse, as well as of different surgical techniques of NCI.

MATERIALS AND METHODS

The outline of the entire developed framework is qualitatively reported in Figure 1: the entire process of analysis involved different tasks, as detailed below.

cMRI acquisitions. Four patients scheduled for surgical repair of IPP due to FED were enrolled in the study (Table 1) at single University Hospital. As per protocol, all patients were in stable preoperative sinus rhythm. These patients , out of 20 contemporary MV P2 prolapse analyzed by cMRI, were chosen because of the different mechanisms underlying a “common functional” isolated P2 prolapse: in detail, patient 1 was affected by the rupture of a single primary chorda arising from posteromedial PM and anchoring on the mid-portion of P2; patient 2 was affected by a triple primary chordal rupture, similarly arising from posteromedial PM and anchoring on mid-P2; patient 3 suffered from a single primary chordal rupture arising from posteromedial PM and anchoring at the “cleft” area of P2 next to P3 scallop; finally patient 4 was affected by a single primary chordal rupture, arising from anterolateral PM and anchoring on mid-P2.

In each preoperative acquisition *cine* cMRI images were acquired on 18 cut-planes evenly rotated around the axis passing through the annular center and aligned with the left ventricle long-axis (Figure 1, panel 1). Thirty cardiac frames were acquired on each plane, with different temporal resolution according to the R-R interval of each patient; cMRI images were acquired using a 3.0T TX Achieva system (Philips Medical System) with a pixel-spacing of 1.25mm and a slice thickness of 8mm.

3D cMRI-derived MV model. The cMRI quantification of MV apparatus was accomplished through a standardized and already published technique.[15] Briefly, the segmentation of the entire set of images was realized using a dedicated software developed in MATLAB (The MathWorks Inc., Natick, MA, United States). The position of reference points, belonging to relevant MV substructures (i.e. mitral annulus, leaflet free margin and papillary muscles), was manually selected within the entire set of images: the coordinates of the identified points were then automatically transformed in the 3D space using the information stored in the appropriate DICOM fields in order to reproduce a complete and patient-specific 3D geometrical model of the MV apparatus. Moreover, the segmentation of the entire set of cine cMRI images allowed to track the motion of both mitral annulus and PMs throughout the entire R-R interval. Relevant parameters were then computed on the basis of the obtained 3D model in order to assess MV geometry at the mid-systolic frame (Table 1).

The initial stress-free MV geometry was reconstructed with reference to end-diastole, i.e. the last frame preceding leaflets closure, and following the approach proposed by Stevanella et al.[15]: a complete 3D model of the mitral apparatus was reconstructed at the selected frame, including the extent of each MV leaflet and the chordal apparatus, defined in accordance to *ex-vivo* findings,[16-18] previous works of the group,[11, 15] and in particular to open-heart surgical appearance. Intraoperative measurements were carried out during surgery in order to assess the length of individual posterior and anterior scallops, height of anterior and posterior commissures. Moreover, the exact location and extent of the prolapsing region were defined and further details concerning IPP lesion were added: i) number and type (1st, 2nd, 3rd order) of the involved chordae; ii) individual rupture or elongation; iii) PM origin of ruptured/elongated chordae; iv) P2-scallop insertion of ruptured/elongated chordae.

Simulation set-up. The simulation set-up was performed as already detailed in previous works.[15] MV 3D numerical models were completed including the mathematical description of the complex mechanical properties of MV leaflets,[19] native chordae tendineae[20] and ePTFE neochordae.[21, 22] All simulations were carried out using the commercial solver ABAQUS Explicit 6.10 (SIMULIA, Dassault Systèmes). MV closure was simulated from end diastole to peak systole, defined as the mid-systolic frame within the R-R interval.

Suture length and neochordal implantation. For each cMRI-derived model, the systolic MV biomechanics was first simulated, reproducing the preoperative scenario of MV lesions and dysfunctions (*Pre-model*). From the *Pre-model*, a physiological MV model (*Phys-model*) was derived, which was characterized by complete and intact chordal apparatus. For the *Phys-model*, the systolic peak configuration was computed, obtaining a physiological level of MV coaptation; based on this configuration, proper suture length was determined for five different NCI procedures, accordingly with the following criteria:

i) Single neochorda implantation (SN, Figure 1, 4a) with suture length approximated in millimeters to the distance (d_P^{Phys}) between the PM tip and the point (P) of neochordal insertion on the MV scallop, as clinically measureable with a surgical caliper;

ii) Double neochorda implantation (DN, Figure 1, 4b) with 2 different sutures arising from the same PM, whose lengths were separately measured as in the SN configuration;

iii) "Standard" neochordal loop (SL, Figure 1, 4c), made of 3 "pre-measured" neochordae of the same length, arising from a loop tightened to a papillary muscle and inserting on the prolapsing leaflet in 3 different points of insertion; neochordal length was set to the maximal distance, in the *Phys-model*, of the selected points from the PM tip;

iv) Non standard "pre-measured" loop (LN, Figure 1, 4d) with a common neochordal loop of 1/3 and 3 different neochordae of 2/3 of the entire (PM tip-to-leaflet free margin) length, determined as in the SL configuration;

v) Non-standard "pre-measured" loop (LNH, Figure 1, 4e), with one neochordal loop of 2/3 and 3 different neochordae of 1/3 of the entire length (LNH), determined as in the SL configuration.

Analyzed parameters. Postoperative systolic function was simulated for each NCI and assessed in terms of the following MV biomechanical parameters which were extracted at peak-systole from FE simulations: i) coaptation area (CoA), defined as the area of the region where the anterior and posterior leaflets overlap after MV closure;[23] ii) coaptation length (CoL) between the anterior and posterior leaflets along the prolapsing region, as routinary assessable through transesophageal echocardiography technology;[24] iii) PM forces (F_{PM}), defined as the resultant reaction force produced by PMs[25] to bear the tension of both native chordae tendinae and ePTFE sutures; iv) native chordal tension (F_{nc}), defined as the sum of forces exerted by native chordae tendinae in the proximity of the prolapsing region; v) artificial chordal tension (F_{ePTFE}) defined as the resultant force exerted by artificial ePTFE neochordae, after NCI; vi) the peak value (S_I^{MAX}) of maximum principal stresses S_I, defined as the maximum value of the tensile stress[26] along the leaflet free margin (i.e. where ePTFE were inserted).

All the above mentioned parameters, with the exception of F_{ePTFE} (since not available in the *Pre-model*), were compared with the corresponding preoperative simulation in order to infer potential biomechanical differences between the performed NCIs. For each patient, the entire set of simulations requested 1 to 2 weeks of computations, and approximately two days of work to segment cMRI data and to carry out the post-processing of computational results.

IRB approved conducting the study and informed consent was obtained from each patient.

RESULTS

Leaflet reposition. In each patient the use of ePTFE sutures, regardless of the performed NCI configuration, concretely repositioned the prolapsing region of the posterior leaflet under the annular plane, all resulting in the disappearance of mitral regurgitation and IPP. Indeed the maximum displacement of free margin along the direction normal to the annular plane (Z relative displacement) was comparable in all the NCI configurations and equal to 9.9±0.4mm in patient 1, 10.8±0.2mm in patient 2, 6.2±0.1mm in patient 3 and 7.3±0.1mm in patient 4, respectively. However, as compared to SN, implantation of multiple neochordae improved the repair in the prolapsing region since a wider realignment of the free margin along the prolapsed P2 region was noticed, as highlighted in the contour maps of leaflet Z relative displacement in NCIs simulations (Figure 1, 4), (i.e the extent of blue areas increased in each postoperative model, while the preoperative leaflet surface is reported in transparent grey color). Moreover, the repaired region of the P2 scallop (i.e. the area of P2 from the midline to the P3) more resembled the morphological configuration of its counterpart segment constituting the P2 scallop (i.e. the area of P2 from the midline to the P1 scallop) at peak systole.

Coaptation area and length. A marked CoA recovery was noticed in all NCIs simulations: however, the best CoA recovery in each patient was achieved with different NCI techniques, according to the anatomy of the disease and the location of the prolapsing region (Table 2, CoA panel). In all patients the lowest CoA recovery was noticed with SN configuration (+22.5% in patient 1, +14.2% in patient 2**,** +3.5% in patient 3 and +19.4% in patient 4, respectively). Throughout the entire set of simulations, the maximal recovery of CoA in each patient was achieved through multiple ePTFE sutures and in particular adopting LN (+33.2%)

and SL (+32.3%) in patient 1, DN (+33.0%) and LNH (+32.6%) in patient 2, LNH (+28.7%) in patient 3, LNH (+20.9%) and SL (+20.7%) in patient 4, respectively.

In the prolapsing region of each preoperative model, CoL was absent due to IPP; a portion of the free margin of the prolapsing scallop thus resulted in no-coaptation as noticeable in Figure 2a.

After NCIs, for each patient, CoL was restored and its mean value was equal to 6.0±0.3mm in patient 1, 6.7±0.4mm in patient 2, 5.4±0.5mm in patient 3 and 7.5±0.2mm in patient 4, respectively; in accordance with CoA-recovery results, the highest CoL values were obtained using multiple NCI: LN (6.41mm) in patient 1, DN (7.15mm) in patient 2, LNH (5.80 mm) in patient 3 and LNH in patient 4 (7.60mm).

PMs forces. In all NCI models, a slight reduction of PM reaction force was noticed (Table 2, F_{PM} panel): in patient 1 and 3 the highest decrease in PM force was measured in the DN configuration (-7.4% and -5.6%, respectively), in patient 2 it was noticed in the LNH configuration (-13.3%) while in patient 4 either in the LNH (-2.5%) or SL (-2.5%) configurations.

Native chordal tension. In all NCI models, chordal tension of the prolapsing region was partially transferred from the intact native chordae to the ePTFE sutures. The reaction forces exerted by the native and intact chordae, adjacent to the prolapsing region, are reported in Table 2 (F_{nc} panel): the range of percentage force reduction was 22÷30%, 32÷43%**,** 17÷35% and 12÷19% for each patient respectively, based on the employed technique. Overall, a decrease in reaction forces was obtained passing from SN to multiple NCIs: the difference in chordal tension F_{nc} between the *Pre-model* and each NCI was highest in LN repair for patient 1 and 2 (0.96N, and 1.71N), in DN repair for patient 3 (1.3N) and in LNH repair for patient 4 (0.49N).

Artificial chordal tension. The force exerted by artificial ePTFE sutures was computed at peak systole for each patient (as detailed in Table 2, F_{ePTFE} panel): although different NCIs were performed, negligible differences in terms of tension were reported on ePTFE sutures (1.04±0.07N in patient 1, 1.47±0.09N in patient 2**,** 0.72±0.06N in patient 3 and 0.79±0.12N in patient 4, respectively).

Stress analysis. In the *Pre-model* of each patient, low S_I stresses were reported on the prolapsing segment of the posterior leaflet; on the contrary, concentrations of S_I stresses were reported in the proximity of the prolapsing region, and in particular: i) along the free margin of P2 scallop close to the insertion of intact native chordae as highlighted in patient 1**,** 2 and 4 (Figure 3, a); ii) on the adjacent posterior scallop P3, as assessable in patient 3, whose prolapse was located in proximity of the P2-P3 "cleft" area. The maximum value of stress S_I^{MAX} was extracted for each *Pre-model*, along the free margin of the posterior leaflet and found to be equal to 272.0kPa, 349.1kPa, 145.6kPa and 364.1kPa, in each patient respectively. In patient 3, S_I stresses were markedly lower compared to other patients; as a matter of fact, the location of prolapse in patient 3 showed to be more lateral (i.e. nearer to P3 scallop) than in the other patients, whose prolapse mainly involved the central P2 scallop.

In postoperative simulations, S_I stresses were computed along the free margin of the entire posterior leaflet and graphically reported in Figure 3b, in order to "spatially" assess and compare the result of different NCIs. Indeed, S_I stresses along the non-prolapsing scallops were substantially unchanged between pre- and post-operative analyses, regardless of the employed technique. On the contrary, S_I stresses noticeably changed on the prolapsing scallop, with postoperative reduction in the areas subtended by native chordae (thus far from the neochordal insertion) - regardless of the employed technique - with a redistribution of S_I stresses at the level of neochordal insertion.

Distribution and magnitude of S_I stresses on neochordal insertion proved to be "technique-specific". In all patients, the highest values of S_1^{MAX} were noticed after implantation of a single neochorda (SN, 270.8kPa, 337.8kPa, 225.8kPa and 267.4kPa for each patient, respectively), while the highest reduction in S_I^{MAX} was achieved through multiple NCI, in particular with LNH in patient 1 (200.6kPa, -26.2% than *Pre-model*), SL in both patient 2 (245.8kPa, -29.6%) and patient 3 (111.4kPa, -23.5%), and LN in patient 4 (223.9kPa, -38.5%). Moreover, in patient 1, 2 and 4, S_1^{MAX} was lower than *Pre-model* for each NCI; on the contrary, only SL configuration achieved a noticeable lower value of S_1^{MAX} with respect to *Pre-model* in patient 3. The values of S_1^{MAX} along the free margin of each model are detailed in Table 2.

In order to assess postoperative distribution of S_I stresses, the contour map of relative variation of S_I stresses (i.e. the difference in S_I stresses between each NCI model and *Pre-model*) is reported for patient 2, at peak systole, in Figure 3c. From a "qualitative" point of view, equivalent patterns of S_I stresses were identified in postoperative simulations, regardless of the employed surgical technique, since in a large area of the P2 scallop stress decreased (green area), thus indicating the unload of native chordae and the relief of excessive mechanical stress on leaflet tissue. In the repaired part of the posterior leaflet, S_l stresses increased after NCI (red area) since ePTFE sutures restored mechanical tension along the prolapsing region of the leaflet: moreover, passing from SN configuration to multiple NCI, the above mentioned progressive decrease in S_l^{MAX} was combined with a larger mechanical redistribution of S_l stresses along the restored part of the MV leaflet.

DISCUSSION

The present study clearly showed, for the first time, that relocation of posterior MV leaflet with different NCI techniques can have different consequences on MV biomechanics, despite comparable "macroscopic" successful surgery, witnessed by the absence of any residual mitral regurgitation and by the restoration of adequate values of CoL and CoA. Furthermore, we were able to demonstrate that biomechanics of prolapsed posterior leaflet change, based on the underlying mechanisms of IPP, and similar changes are noticeably postoperatively, in a "technique-specific" fashion. Finally we report that – through an integrated bioengineer-radiological-surgical approach to the simulation of MV apparatus - reliability of FE analysis clearly increases, with the potential for both an elegant reproduction of different surgical repairs and a detailed definition of the postoperative biomechanical changes associated to several NCI techniques.

According to our data, it is possible to define in any patient a theoretical patient-specific "gold standard" NCI technique, in terms of both "macroscopic" and "biomechanical" characteristics. Indeed, coaptation area (CoA) and length (CoL) can be considered as "macroscopic" pivotal parameters (as a matter of fact, surgery generally aims at maximizing both parameters): however, "biomechanical" variables, such as the relief of tension on the native chordae, the degree of stress redistribution on MV leaflets, and peak mechanical stresses observed along the leaflet free margin after NCI, although not directly measureable by surgeons, may play a crucial role in defining the "best repair technique". As examples, in patients 1 and 4 (who shared a similar but "specular" mechanism of isolated P2 prolapse), LN and LNH respectively proved to be the best available surgical options, because they individually combine the highest recovery of CoA and CoL with the highest relief of tension on the native chordae (F_{nc}), leaving substantially unchanged the reaction forces of the papillary muscle (F_{PM}) and achieving also significant reduction of S_l^{MAX} along the free margin. According to these findings, it can also be argued that a correlation between FE-derived biomechanics at the time of the repair and clinical long-term follow-up of different techniques of NCIs (e.g. via a recurrence of MV regurgitation) may help to elucidate which of the considered biomechanical variables might play a crucial role in the fate of MV repair. Indeed, sporadic primary failure of ePTFE neochordae, as well as several case reports of neochoral calcification and fracture, have been reported in the literature.[27, 28]

Postoperative changes in MV biomechanics assessed with cMRI-derived FE models can represent a valuable background to deeper understand the biomechanical implications following the surgical repair. It is worth of noting that preoperative stresses are usually concentrated on the leaflet areas next to the prolapse (as graphically reported in Figure 3); moreover, these stresses might have acted, with their potential weakening effect, on those areas for a long time before repair. Therefore, despite we reported that all the NCI techniques transferred-back these stresses on the prolapsed area (indeed clinical practice with NCI is almost always a successful story), adjacent areas may remain weak, being the potential initial source for a future relapse of IPP (possibly due also to a more rapid progression of the remodeling processes of MV degeneration, triggered by the long-lasting stresses on these areas). Indeed, it is common practice to re-operate patients with recurrent mitral leaflet prolapse without evidence of NCI failure, as reported in most clinical series.[8, 29] These data could suggest that multiple neochordal stitching involving also the areas next to the prolapsed region, although unusual in current surgical practice, might be considered in order to reinforce those chronically weakened areas adjacent to the prolapsed region, thus potentially ameliorating long-term clinical results.

Indeed, our cMRI-derived FE models confirmed the clinical hypothesis,[9, 30] according to which multiple ePTFE neochordae can provide a larger leaflet coaptation area, better preserve the ventriculo-annular continuity, and better redistribute stresses on the repaired leaflet. As clinically supposed, in our simulations the largest CoA and the highest reduction of S_l^{MAX} along the free margin were achieved with multiple NCI. As for patients 1, 2 and 4, also patient 3 reported a progressive decline of S_l^{MAX} along the free margin passing from SN to loop-techniques. However, the unexpected increase, with respect to *Pre-model*, in S_I^{MAX} of LN (+29.8%) and LNH (+23.0%) in patient 3, compared to its reduction only with SL configuration (-23.5%), deserves further speculations. We hypothesized that it can be related to a higher spatial flexibility - compared to a relatively "more constraining" effect with LN and LNH configurations - offered by the SL configuration, where artificial neochordae can better adapt to the postoperative geometry, thus achieving a more physiological redistribution of stresses along both P2 and P3 free margins. Certainly, future studies are needed to further investigate the peculiar biomechanics of para-medial P2-prolapse and to confirm these preliminary speculations.

In conclusion, FE patient-specific simulations highlighted biomechanical differences in the outcome of several NCI configurations: the performed tests may potentially impact the clinical outcome of the procedure and promote, if extensively and successfully tested, a patient-specific optimization of NCI techniques for the treatment of degenerative MV prolapse. As compared to, e.g., transesophageal echocardiography, cMRI implies higher costs and less convenience. However, it allows for a more reliable 3D reconstruction of the morphology of the entire mitral apparatus, and of the complete kinematics of its substructures. The impact of valve morphology and kinematic boundary conditions on the computed biomechanical variables [31] led to the use of a cMRI-based modeling approach.

Limitations.

The present study has three main limitations.

First, it is based on the analysis of a small cohort of patients with IPP. However, according to the speculative purpose of the study, each anatomical substrate served as benchmark for biomechanical tests on five different surgical NCI techniques.

Second, to date there is no "evident clinical proof" of a biomechanical-induced relapse of IPP, since we do not have any long-term follow up data referred to the analyzed patients. As a consequence, we cannot translate our quantitative results, which are referred to an acute post-operative condition, into long-term prognostic indicators.

Third, the adopted modeling methodology requires a consistent amount of computational and human work, which is not compatible with its use for a routine clinical application.

Accordingly, in order to overcome all the above mentioned limitations, future efforts will be focused on further expansion of these preliminary results through the enrollment of more patients, as well as on their monitoring over a long-term follow-up. Also, in order to develop more clinically-oriented tools, we are already exploring different modeling approaches that, at the cost of a less detailed quantification of biomechanical variables (i.e. local strains and stresses), allow for very fast and almost real-time simulations.[32] Finally, increasing the cohort of enrolled patients will provide an improved correlation between biomechanical differences and clinical outcomes of different surgical techniques and help to stratify, on the basis of a larger range of MV prolapse patterns, potential clinical risks associated with some MV repairs.

FIGURES

FIGURE 1. Workflow of the study: procedure of manual segmentation (1) and computational modeling (2) for a patient-specific MV preoperative geometry with IPP; simulation of *Phys-model* (3) and different NCIs with proper determination of each suture length (4); as example, the contour map of Z relative displacement is reported at peak systole on the posterior leaflet, for each NCI postoperative simulation in patient 2 (ePTFE sutures are generally visualized with a spring-like appearance).

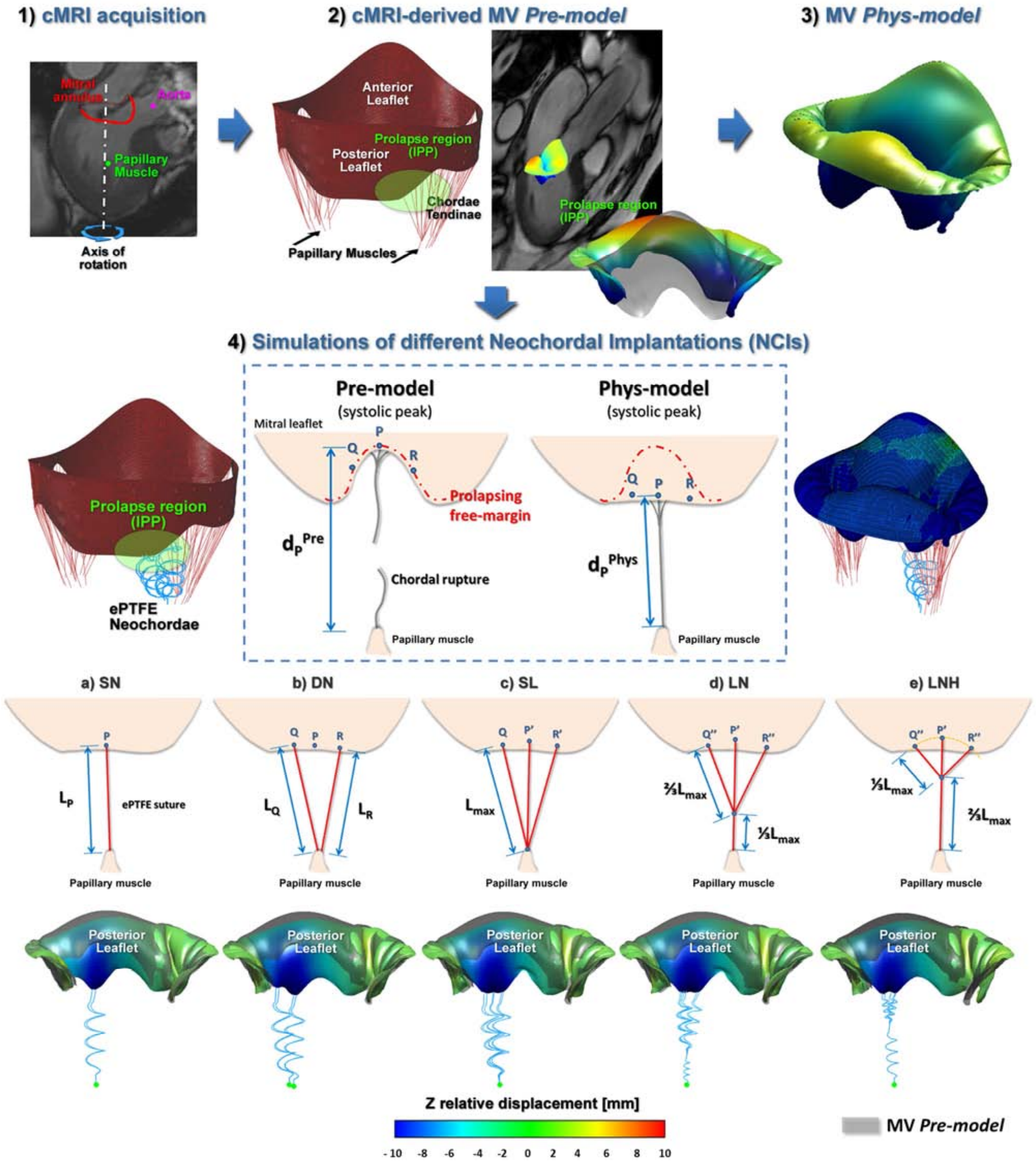

FIGURE 2. Coaptation length (CoL) on the prolapsing posterior leaflet of patient 2 *Pre-model* (a); coaptation area (a) in each *Pre-model* (for each patient, the arrow indicates the region of no-coaptation due to leaflet prolapse); coaptation length (CoL) on the posterior leaflet of patient 2 after NCI (c, SL configuration); contour maps of CoA (reported in green) after NCIs, for each patient, respectively (d).

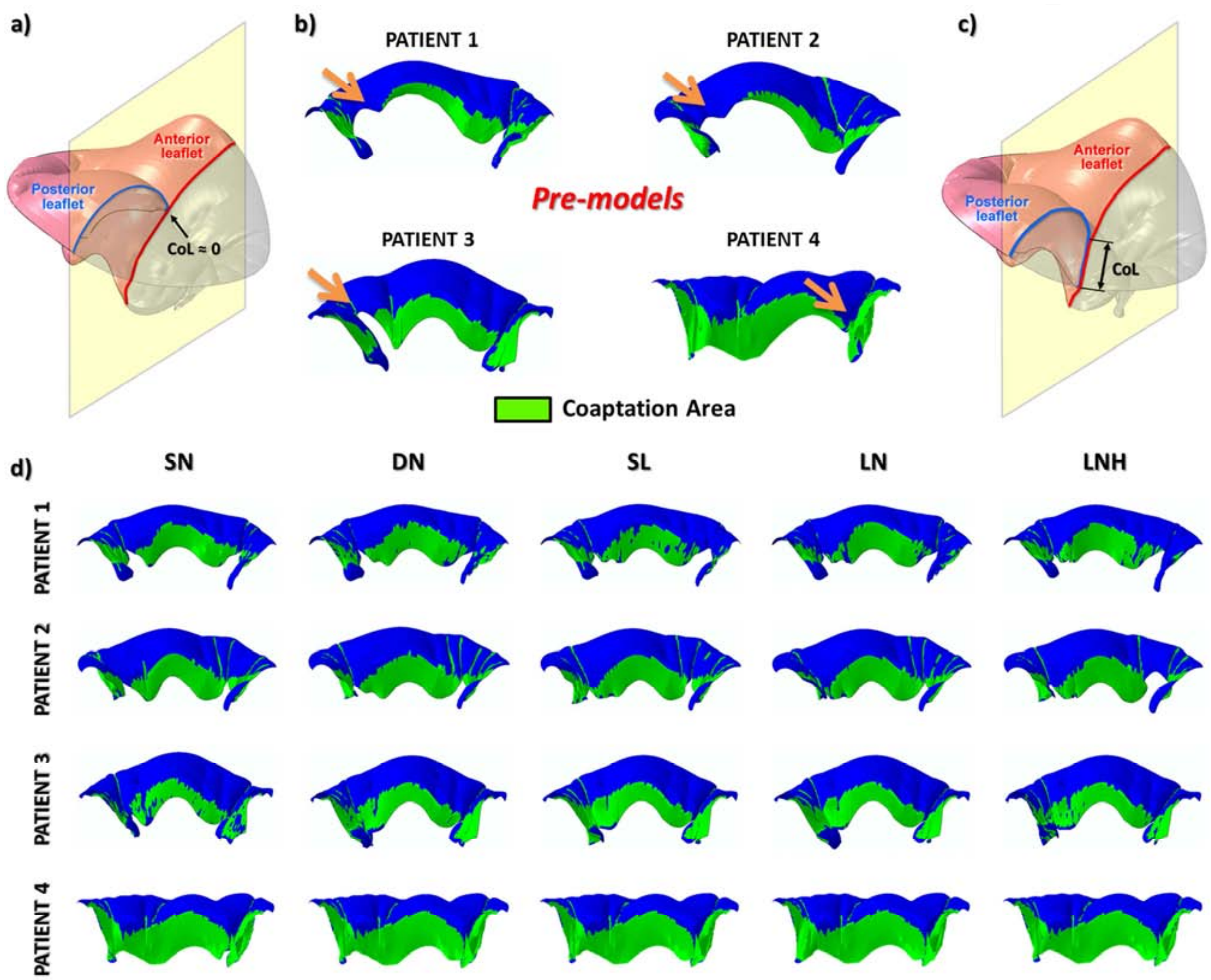

FIGURE 3. Results of stress analysis: a) Contour map of S_I stresses in the preoperative conditions for each patient (*Pre-models*); b) spatial distribution of S_I stress along the free margin of the posterior mitral scallops (P1, P2 and P3 respectively); c) Contour map of relative S_I stresses variation, between each NCI model and *Pre-model*, in patient 2.

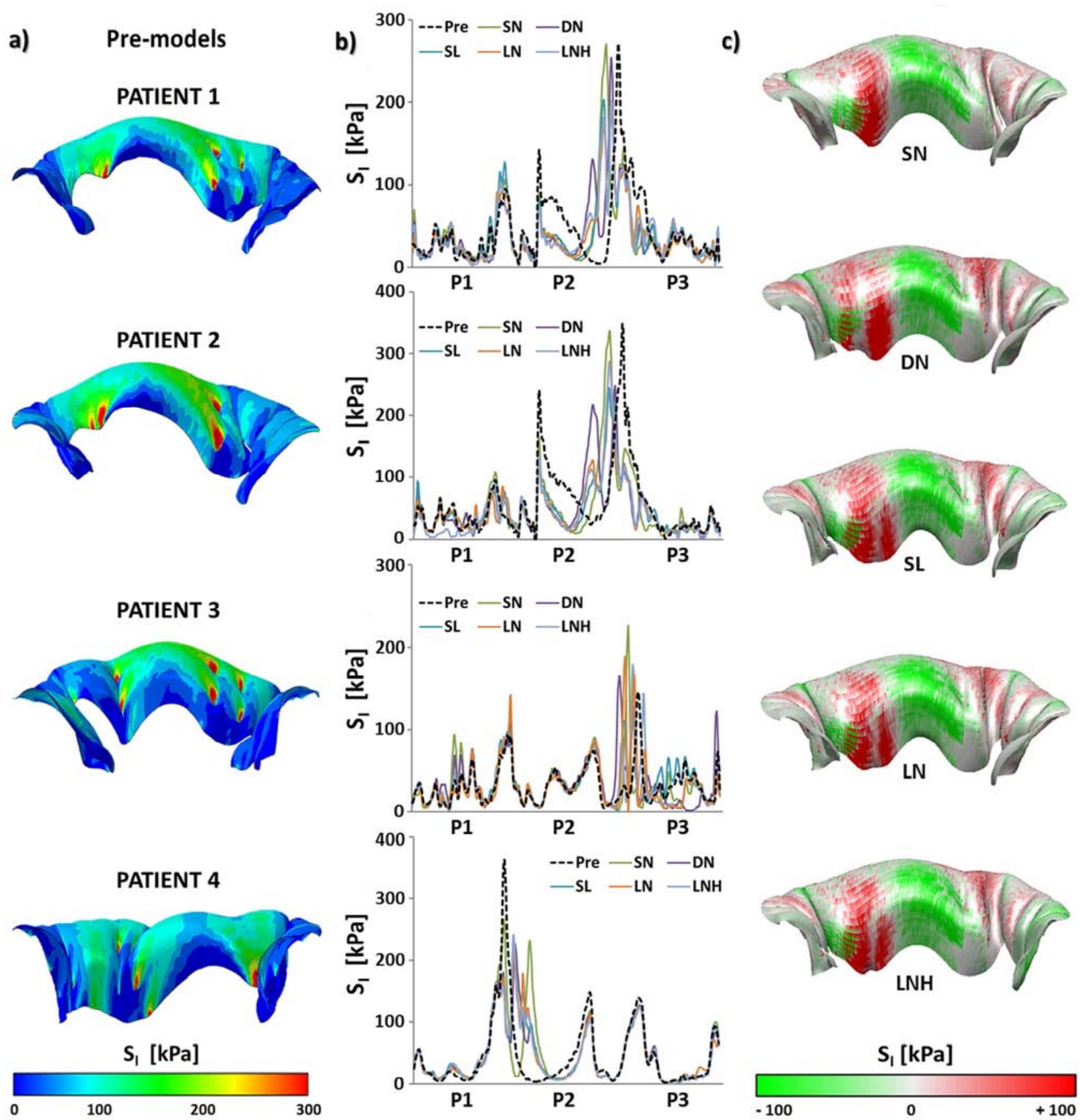

TABLES

TABLE 1. General characteristics of enrolled patients

	Patient 1	**Patient 2**	**Patient 3**	**Patient 4**
Gender	F	M	F	F
Age (years)	77	75	76	80
Weight (kg)	75	83	60	65
Height (cm)	160	168	160	162
BSA (m^2)	1.78	1.93	1.62	1.69
Heart Rate (bpm)	63	88	65	62
A2D/BSA (cm^2/m^2)	6.55	5.96	8.97	8.78
D_{SL} (mm)	30.5	32.8	37.2	40.6
D_{CC} (mm)	40.9	43.3	45.7	46.5
e (-)	1.34	1.32	1.23	1.14
IPP region	P2	P2	P2-P3	P2

BSA=Body Surface Area; A2D=annular area projection on MV plane; D_{SL}=septo-lateral diameter; D_{CC}=commissural diameter; e=eccentricity (D_{CC}/D_{SL}); IPP region= main prolapsing scallop in the posterior MV leaflet.

TABLE 2. Computed coaptation areas (CoAs), coaptation lengths in the prolapsing region (CoLs), native chordae tensions in the prolapsing region (F_{nc}), ePTFE neochordae tensions (F_{ePTFE}), PM reaction forces (F_{PM}) and peak value of S_I stresses (S_I^{MAX}) along the posterior free margin in preoperative models (IPP, where available) and after different NCIs[1]

		Patient 1	Patient 2	Patient 3	Patient 4
CoA [mm^2]	IPP	129.7	203.1	176.1	204.5
	SN	159.0 (+22.5%)	232.0 (+14.2%)	182.3 (+3.5 %)	244.2 (+19.4 %)
	DN	159.5 (+23.0%)	270.1 (+33.0%)	220.6 (+25.3 %)	244.9 (+19.7 %)
	SL	171.6 (+32.3%)	259.7 (+27.8%)	215.7 (+22.5 %)	246.8 (+20.7 %)
	LN	172.8 (+33.2%)	246.8 (+21.5%)	204.0 (+15.9%)	245.7 (+20.1 %)
	LNH	164.7 (+27.0%)	269.3 (+32.6%)	226.6 (+28.7%)	247.3 (+20.9 %)
CoL [mm]	IPP	-	-	-	-
	SN	5.74	6.17	4.57	7.19
	DN	5.71	7.15	5.78	7.48
	SL	6.25	6.73	5.44	7.58
	LN	6.41	6.56	5.47	7.53
	LNH	5.94	6.99	5.80	7.60
F_{nc} [N]	IPP	3.21	3.99	3.72	2.56
	SN	2.50 (-22.2%)	2.70 (-32.4%)	2.89 (-22.2%)	2.25 (-11.8%)
	DN	2.34 (-27.2%)	2.41 (-39.6%)	2.42 (-34.9%)	2.16 (-15.6%)
	SL	2.41 (-24.9%)	2.38 (-40.4%)	3.09 (-17.0%)	2.09 (-18.3%)
	LN	2.25 (-29.9%)	2.28 (-42.9%)	2.63 (-29.4%)	2.09 (-18.3%)
	LNH	2.26 (-29.7%)	2.42 (-39.4%)	2.60 (-30.1%)	2.07 (-19.1%)
F_{ePTFE} [N]	IPP	-	-	-	-
	SN	0.94	1.31	0.65	0.59
	DN	1.06	1.54	0.76	0.75
	SL	1.00	1.50	0.67	0.86
	LN	1.07	1.48	0.78	0.87
	LNH	1.12	1.53	0.76	0.88
F_{PM} [N]	IPP	14.08	13.58	15.48	17.57
	SN	13.39 (-4.9%)	12.42 (-8.6%)	14.77 (-4.6%)	17.22 (-2.0%)
	DN	13.04 (-7.4%)	12.15 (-10.5%)	14.62 (-5.6%)	17.16 (-2.4%)
	SL	13.22 (-6.1%)	12.20 (-10.2%)	15.36 (-0.8%)	17.14 (-2.5%)
	LN	13.11 (-6.9%)	12.15 (-10.5%)	15.02 (-2.9%)	17.16 (-2.4%)
	LNH	13.16 (-6.5%)	11.78 (-13.3%)	15.06 (-2.7%)	17.14 (-2.5%)
S_I^{MAX} [kPa]	IPP	272.0	349.1	145.6	364.1
	SN	270.8 (-0.4 %)	337.8 (-3.2 %)	225.8 (+55.1 %)	267.4 (-26.6 %)
	DN	254.5 (-6.5 %)	248.7 (-28.8 %)	165.1 (+13.4 %)	227.2 (-37.6 %)
	SL	202.7 (-25.5 %)	245.8 (-29.6 %)	111.4 (-23.5 %)	231.6 (-36.4 %)
	LN	201.1 (-26.1 %)	287.9 (-17.5 %)	189.1 (+29.8 %)	223.9 (-38.5 %)
	LNH	200.6 (-26.2 %)	284.8 (-18.4 %)	179.1 (+23.0 %)	242.4 (-33.4 %)

[1] Percentage variations with respect to IPP models are reported in brackets

References

1. Iung B, Baron G, Butchart EG, Delahaye F, Gohlke-Barwolf C, Levang OW, et al. A prospective survey of patients with valvular heart disease in Europe: The Euro Heart Survey on Valvular Heart Disease. *Eur Heart J.* 2003;24:1231-43.
2. Carpentier A. Cardiac valve surgery--the "French correction". *J Thorac Cardiovasc Surg.* 1983;86:323-37.
3. Perier P, Hohenberger W, Lakew F, Batz G, Urbanski P, Zacher M, et al. Toward a new paradigm for the reconstruction of posterior leaflet prolapse: midterm results of the "respect rather than resect" approach. *Ann Thorac Surg.* 2008;86:718-25.
4. Calafiore AM. Choice of artificial chordae length according to echocardiographic criteria. *Ann Thorac Surg.* 2006;81:375-7.
5. Duran CM, Pekar F. Techniques for ensuring the correct length of new mitral chords. *J Heart Valve Dis.* 2003;12:156-61.
6. Mandegar MH, Yousefnia MA, Roshanali F. Preoperative determination of artificial chordae length. *Ann Thorac Surg.* 2007;84:680-2.
7. Adams DH, Kadner A, Chen RH. Artificial mitral valve chordae replacement made simple. *Ann Thorac Surg.* 2001;71:1377-8.
8. Salvador L, Mirone S, Bianchini R, Regesta T, Patelli F, Minniti G, et al. A 20-year experience with mitral valve repair with artificial chordae in 608 patients. *J Thorac Cardiovasc Surg.* 2008;135:1280-7.
9. Scorsin M, Al-Attar N, Lessana A. A novel technique of utilizing artificial chordae for repair of mitral valve prolapse. *J Thorac Cardiovasc Surg.* 2007;134:1072-3.
10. Adams DH, Anyanwu AC, Rahmanian PB, Filsoufi F. Current concepts in mitral valve repair for degenerative disease. *Heart Fail Rev.* 2006;11:241-57.
11. Votta E, Le TB, Stevanella M, Fusini L, Caiani EG, Redaelli A, et al. Toward patient-specific simulations of cardiac valves: state-of-the-art and future directions. *Journal of biomechanics.* 2013;46:217-28.
12. Reimink MS, Kunzelman KS, Cochran RP. The effect of chordal replacement suture length on function and stresses in repaired mitral valves: a finite element study. *J Heart Valve Dis.* 1996;5:365-75.
13. Kunzelman K, Reimink MS, Verrier ED, Cochran RP. Replacement of mitral valve posterior chordae tendineae with expanded polytetrafluoroethylene suture: a finite element study. *J Card Surg.* 1996;11:136-45.
14. Rim Y, Laing ST, McPherson DD, Kim H. Mitral valve repair using ePTFE sutures for ruptured mitral chordae tendineae: a computational simulation study. *Ann Biomed Eng.* 2014;42:139-48.
15. Stevanella M, Maffessanti F, Conti CA, Votta E, Arnoldi A, Lombardi M, et al. Mitral Valve Patient-Specific Finite Element Modeling from Cardiac MRI: Application to an Annuloplasty Procedure. *Cardiovascular Engineering and Technology.* 2011;2:66-76.
16. Lam JH, Ranganathan N, Wigle ED, Silver MD. Morphology of the human mitral valve. I. Chordae tendineae: a new classification. *Circulation.* 1970;41:449-58.
17. Ranganathan N, Lam JH, Wigle ED, Silver MD. Morphology of the human mitral valve. II. The value leaflets. *Circulation.* 1970;41:459-67.
18. Degandt AA, Weber PA, Saber HA, Duran CM. Mitral valve basal chordae: comparative anatomy and terminology. *Ann Thorac Surg.* 2007;84:1250-5.
19. May-Newman K, Yin FC. A constitutive law for mitral valve tissue. *J Biomech Eng.* 1998;120:38-47.
20. Kunzelman KS, Cochran RP. Mechanical properties of basal and marginal mitral valve chordae tendineae. *ASAIO Trans.* 1990;36:M405-8.

21. Dang MC, Thacker JG, Hwang JC, Rodeheaver GT, Melton SM, Edlich RF. Some biomechanical considerations of polytetrafluoroethylene sutures. *Arch Surg.* 1990;125:647-50.
22. Votta E, Paroni L, Conti CA, Pelosi A, Mangini A, D'Alesio P, et al. Aortic Valve Repair via Neo-Chordae Technique: Mechanistic Insight Through Numerical Modelling. *Ann Biomed Eng.* 2012;40:1039-51.
23. Maffessanti F, Marsan NA, Tamborini G, Sugeng L, Caiani EG, Gripari P, et al. Quantitative analysis of mitral valve apparatus in mitral valve prolapse before and after annuloplasty: a three-dimensional intraoperative transesophageal study. *Journal of the American Society of Echocardiography : official publication of the American Society of Echocardiography.* 2011;24:405-13.
24. Gogoladze G, Dellis SL, Donnino R, Ribakove G, Greenhouse DG, Galloway A, et al. Analysis of the mitral coaptation zone in normal and functional regurgitant valves. *The Annals of Thoracic Surgery.* 2010;89:1158-61.
25. Vismara R, Pavesi A, Votta E, Taramasso M, Maisano F, Fiore GB. A pulsatile simulator for the in vitro analysis of the mitral valve with tri-axial papillary muscle displacement. *The International journal of artificial organs.* 2011;34:383-91.
26. Ragab A-RA, Bayoumi SEA. *Engineering Solid Mechanics: Fundamentals and Applications*. Boca Raton, Florida: CRC Press; 1998.944.
27. Coutinho GF, Carvalho L, Antunes MJ. Acute mitral regurgitation due to ruptured ePTFE neo-chordae. *J Heart Valve Dis.* 2007;16:278-81.
28. Butany J, Collins MJ, David TE. Ruptured synthetic expanded polytetrafluoroethylene chordae tendinae. *Cardiovasc Pathol.* 2004;13:182-4.
29. Kobayashi J, Sasako Y, Bando K, Minatoya K, Niwaya K, Kitamura S. Ten-year experience of chordal replacement with expanded polytetrafluoroethylene in mitral valve repair. *Circulation.* 2000;102:III30-4.
30. Falk V, Seeburger J, Czesla M, Borger MA, Willige J, Kuntze T, et al. How does the use of polytetrafluoroethylene neochordae for posterior mitral valve prolapse (loop technique) compare with leaflet resection? A prospective randomized trial. *J Thorac Cardiovasc Surg.* 2008;136:1205; discussion -6.
31. Stevanella M, Votta E, Redaelli A. Mitral valve finite element modeling: implications of tissues' nonlinear response and annular motion. *J Biomech Eng.* 2009;131:4000107.
32. Hammer PE, Sacks MS, del Nido PJ, Howe RD. Mass-spring model for simulation of heart valve tissue mechanical behavior. *Ann Biomed Eng.* 2011;39:1668-79.

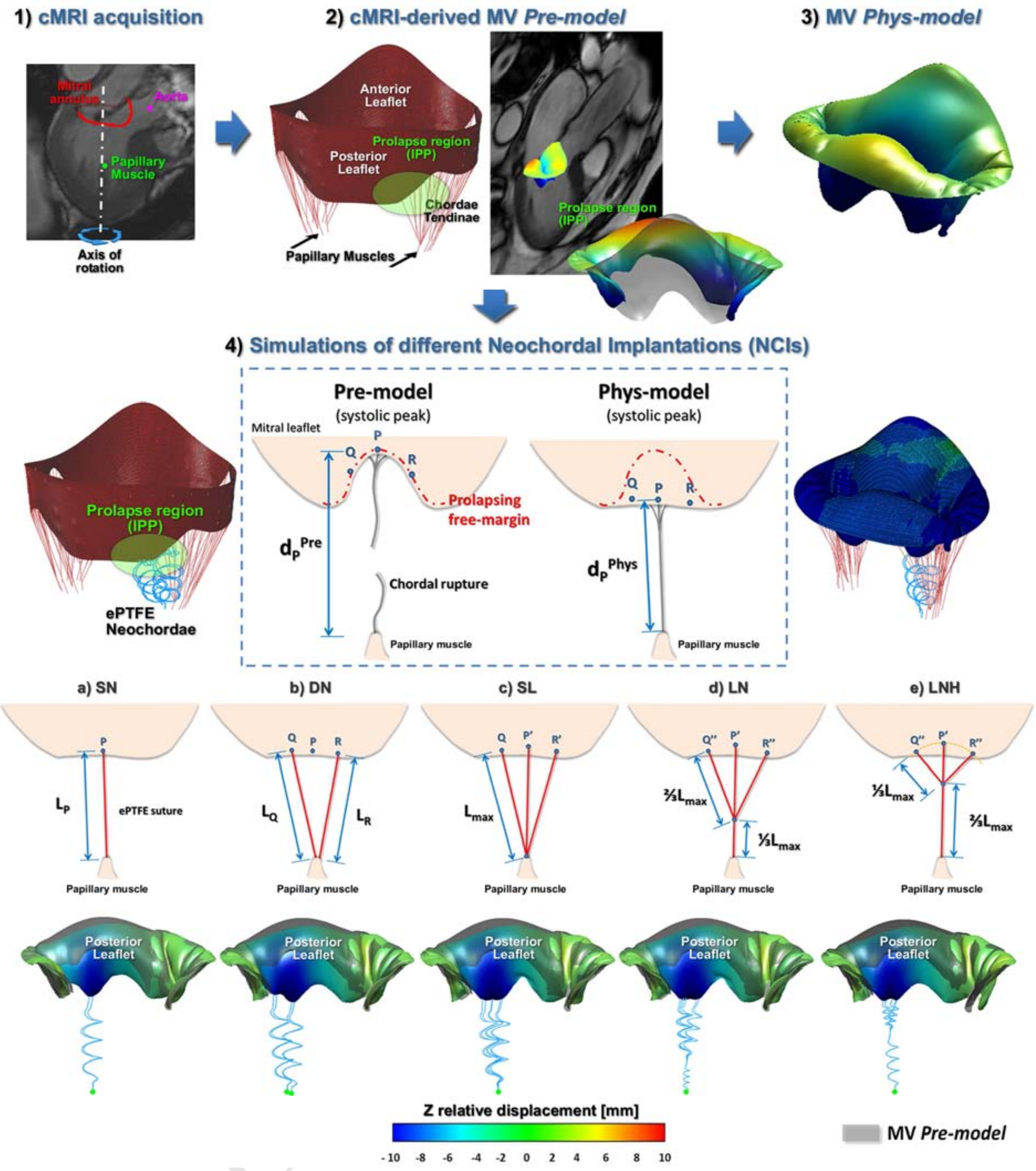
1) cMRI acquisition
Mitral annulus
Aorta
Papillary Muscle
Axis of rotation
2) cMRI-derived MV Pre-model
Anterior Leaflet
Posterior Leaflet
Prolapse region (IPP)
Chordae Tendinae
Papillary Muscles
3) MV Phys-model
4) Simulations of different Neochordal Implantations (NCIs)
Prolapse region (IPP)
ePTFE Neochordae
Pre-model
(systolic peak)
Mitral leaflet
Prolapsing free-margin
Chordal rupture
Papillary muscle
Phys-model
(systolic peak)
a) SN
b) DN
c) SL
d) LN
e) LNH
ePTFE suture
Papillary muscle
Posterior Leaflet
Z relative displacement [mm]
-10 -8 -6 -4 -2 0 2 4 6 8 10
MV Pre-model

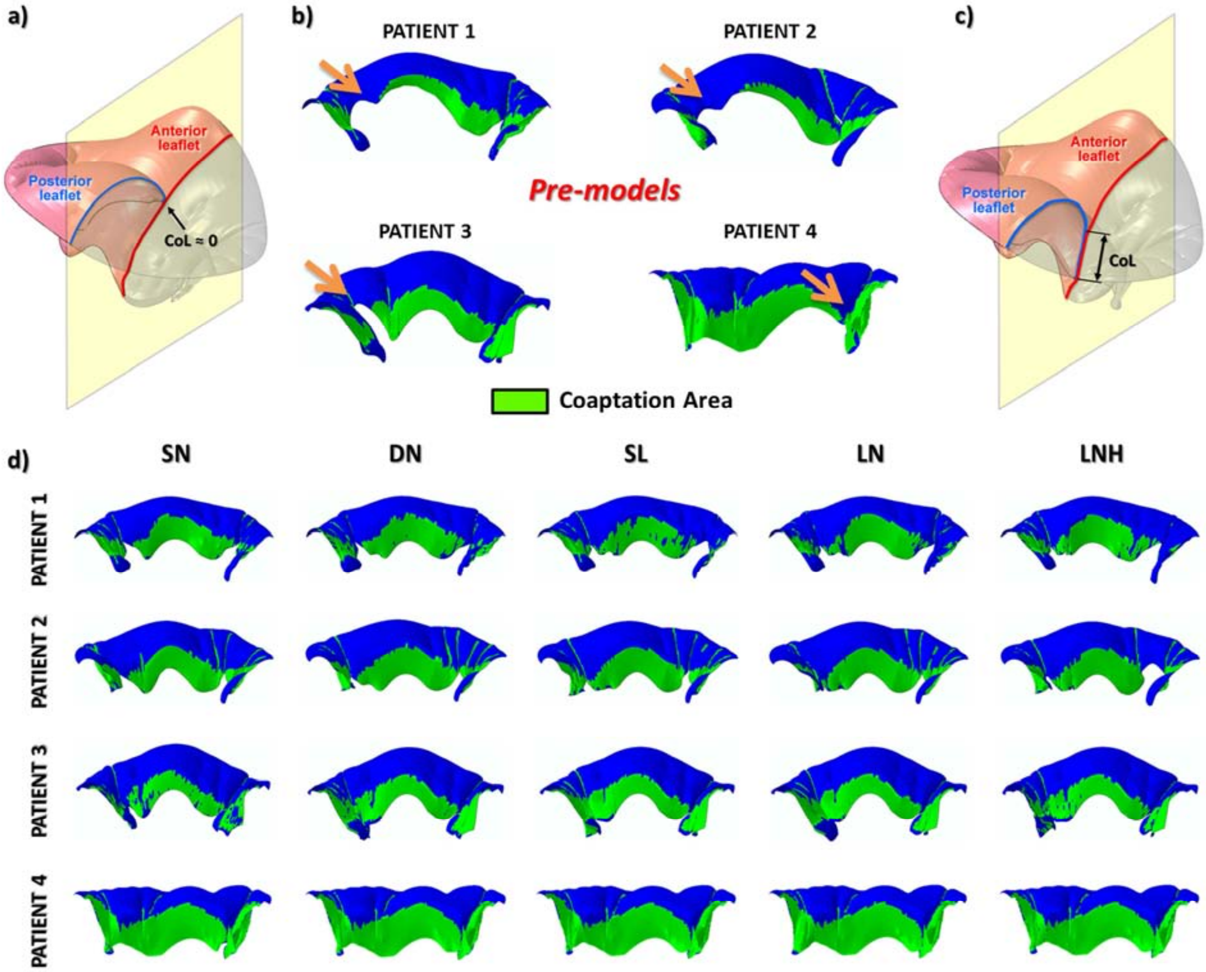
a)
Anterior leaflet
Posterior leaflet
CoL ≈ 0
b)
PATIENT 1
PATIENT 2
Pre-models
PATIENT 3
PATIENT 4
Coaptation Area
c)
Anterior leaflet
Posterior leaflet
CoL
d)
SN
DN
SL
LN
LNH
PATIENT 1
PATIENT 2
PATIENT 3
PATIENT 4

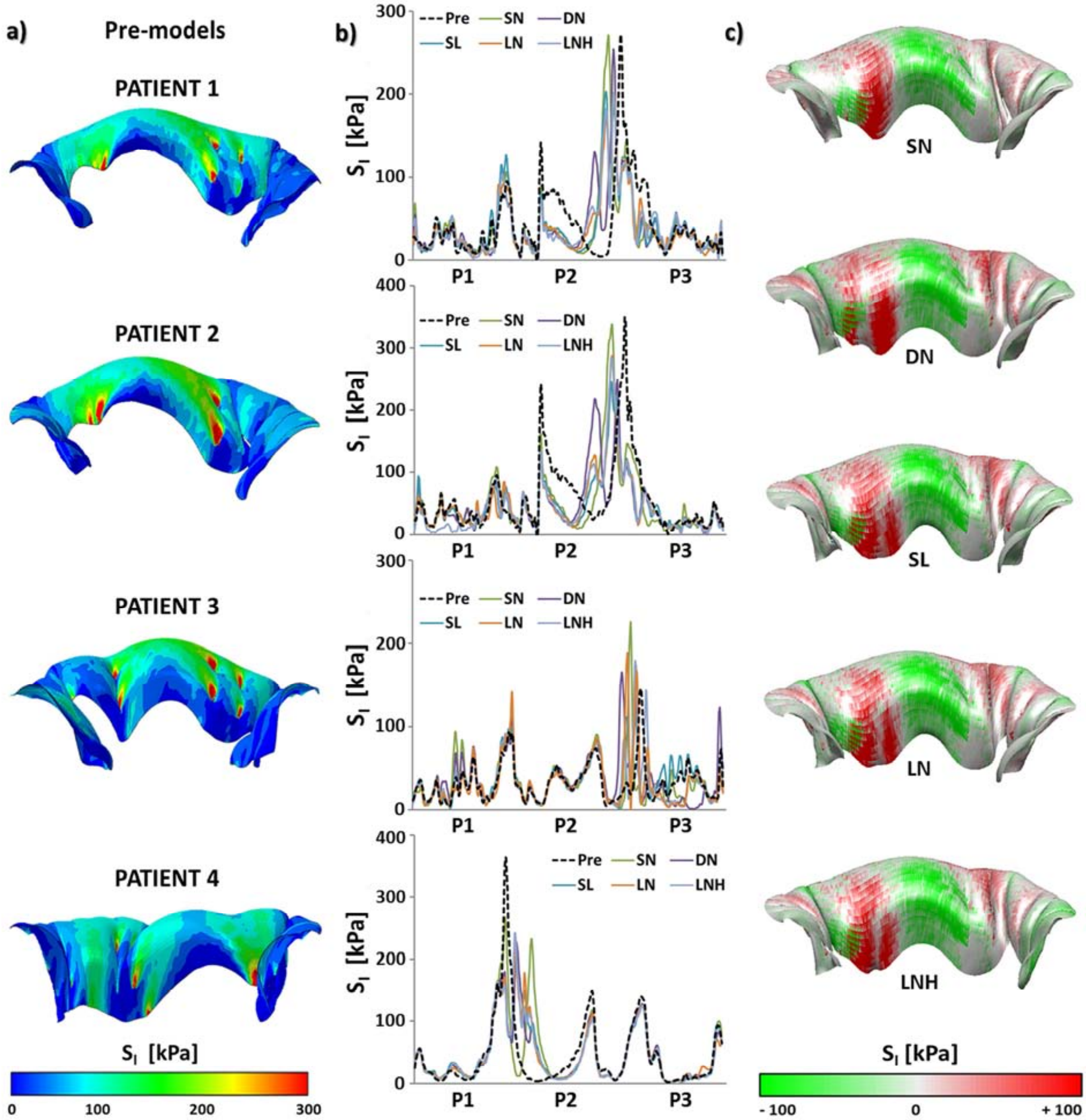
a)
Pre-models
PATIENT 1
PATIENT 2
PATIENT 3
PATIENT 4
S_I [kPa]
0
100
200
300
b)
Pre
SN
DN
SL
LN
LNH
S_I [kPa]
P1
P2
P3
c)
SN
DN
SL
LN
LNH
S_I [kPa]
- 100
0
+ 100